J. Fluid Mech. (1989). *vol.* 204, *pp.* 167–184
Printed in Great Britain

Image processing of the near wakes of stationary and rotating cylinders

By J. MASSONS, X. RUIZ AND F. DÍAZ

Laboratori de Física Aplicada, Dept. Química, University of Barcelona,
P. Imperial Tarraco, 1, 43005 Tarragona, Catalunya, Spain.

(Received 5 April 1988 and in revised form 23 January 1989)

Statistical properties of the position of the turbulent/non-turbulent interface in the near wake of stationary and spinning cylinders have been measured for $Re = 2000$, using image processing techniques. The results include the first statistical moments, intermittency and burst-rate profiles, auto- and cross-correlation functions, auto- and cross-spectra and phase spectra. They indicate that the rotation of the cylinder causes substantial changes in the structure of the flow.

1. Introduction

In spite of the apparent simplicity of the wake generated by a cylinder, this flow has been, and still is, one of the most studied systems in the literature (Townsend 1949; Roshko 1953; Schlichting 1958; Tritton 1959; Keffer 1965; Gerrard 1966; Charrier 1979; Browne & Antonia 1986; Freymuth, Finaish & Bank 1986; Lim & Sirovich 1986; Eaton 1987; Jackson 1987; Kourta *et al.* 1987.) This is because of the large variety and complexity of phenomena developed in it and, at the same time, to the numerous technological situations in which this kind of flow occurs. Cylinder rotation makes substantial changes in the wake with respect to the stationary case and, at the same time, involves important practical applications as a consequence of the Magnus effect and the decreasing of the drag coefficient (Díaz *et al.* 1983).

The generation of the pseudo-deterministic vortices in a stationary cylinder wake is a consequence of the instability of the two shear layers resulting from the upper and lower boundary layer detachment. Rotation of the cylinder produces different lateral velocity gradients in the regions above and below the cylinder, which imply modifications to the process that governs the formation of the Kármán vortices, especially when the peripheral velocity of the cylinder, U_p, increases beyond the free-stream velocity, U_0. The decay of the Kármán vortex activity and the increase in the random modulation of the shedding process is linked to the displacement of the stagnation point and to the thickening of the layer of rotating fluid near the cylinder surface, which cause separation to occur progressively away from the surface of the cylinder. Also, as $\lambda \equiv U_p/U_0$ increases, the mean velocity profiles become increasingly asymmetrical and the lateral position of the maximum velocity defect is laterally displaced in a direction consistent with the sense of the cylinder rotation (Díaz *et al.* 1985).

The study carried out by Shokr & Keffer (1982) in the near wake of two closely spaced circular cylinders has suggested that the statistics of the interface differ substantially from Gaussian behaviour. These differences diminish with increasing distance from the cylinder, and the results of LaRue & Libby (1976) show that the

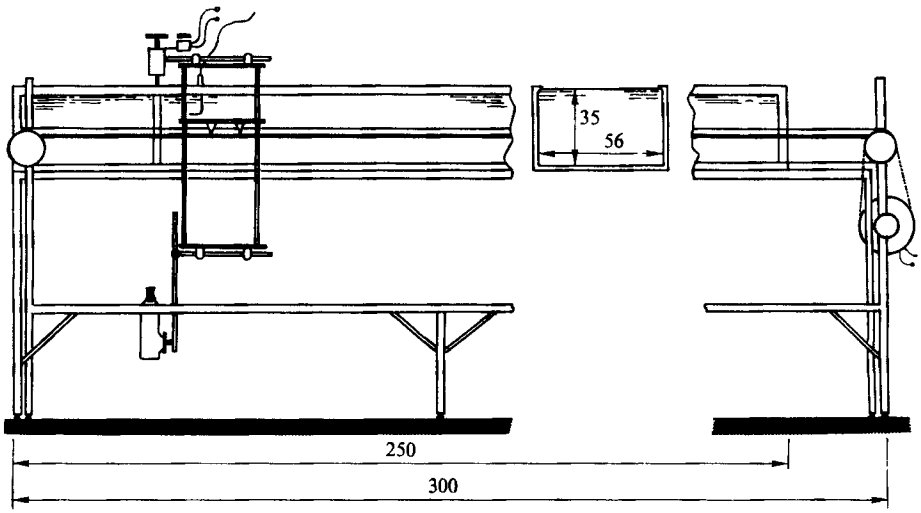

FIGURE 1. Sketch of the towing water tank.

statistics governing the interface in a fully developed turbulent cylinder wake become Gaussian because of decreasing coherence of the flow structures.

In this work, the turbulent/non-turbulent interface in the near wake of stationary and rotating cylinders is studied for moderate Reynolds number ($Re = 2000$). The location of the interface is obtained by applying image processing techniques to visualizations of the flow using dye injection.

In recent years, there has been considerable interest in these techniques (Nagib *et al.* 1978; Sadjadi *et al.* 1980; Hernán & Jiménez 1982; Hesselink & White 1983; Kobayashi *et al.* 1985; Marko & Rimai 1985; Massons *et al.* 1986; Hesselink 1988; Prasad & Sreenivasan 1989). The present work concentrates on the instantaneous position of the turbulent/non-turbulent interface because of its importance in the entrainment process. The interface position is usually determined by means of the analysis of instantaneous anemometric (Antonia & Bradshaw 1971; Thomas 1973) or thermoanemometric signals (Sreenivasan & Tavoularis 1980; Rajagopalan & Antonia 1981). The technique used in this paper is an alternative method which also allows a complete statistical study of the turbulent/non-turbulent interface.

2. Experimental details

The flow visualization experiments were done in a towing water tank of 56×35 cm in section and 250 cm in length, which is fully described by Massons (1987). Figure 1 shows a sketch of the equipment. A guide-rail system, on which a carriage moved, carries the model, the lighting system and the cinematographic recording camera. The illumination of the observation plane is obtained by two movie lights, each of 1000 W, situated on both sides of the tank and collimated by a 5 mm wide slit. The visualizations were recorded on a Kodak Ektachrome 160 S/8 cinematographic film at 24 frames per second. The model used was a cylinder of diameter $D = 3$ cm (blockage ratio 0.053). The velocity of the carriage was 6.6 cm s^{-1}, which produced a cylinder Reynolds number of about 2000. A definition sketch of the flow analysed is shown in figure 2. The length-to-diameter ratio was more than 10, so that the

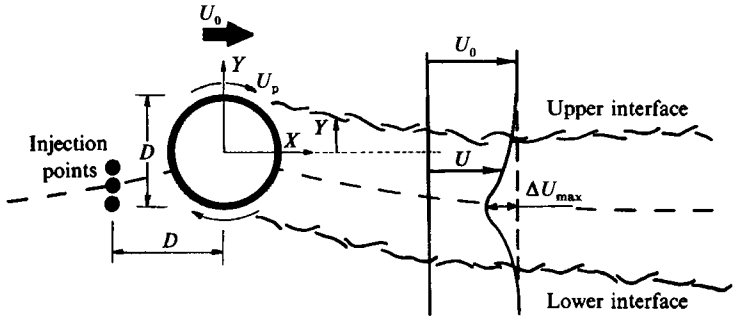

FIGURE 2. Definition sketch.

statistical properties of the flow were effectively functions of the X- and Y-coordinates only (i.e. the wake was two-dimensional). The cylinder was connected to a variable-speed motor so that it could be rotated at selected peripheral speeds, U_p, up to 4 times the free-stream velocity, U_0. To visualize the flow, silicone oil was used, suitably mixed with salted water in order to adjust its density to that of the water used. The dye is injected at the level of the illumination plane by a rake of three L-shaped parallel tubes of 0.8 mm in diameter. The injection points are located one diameter upstream from the cylinder, as indicated in figure 2. Figure 3(*a–f*) shows photographic copies of six frames of the cine film, as an example of the different wakes analysed in this work.

3. Image processing procedures

Cine pictures were digitized using a Bosch monochromatic video camera, which allows a resolution of 512×512 pixels with 256 grey levels per pixel. The minimum distance resolved is $\frac{1}{58}$ of the cylinder diameter. A record of 25 s was studied for each case. Digital image processing was carried out on IBAS/IPS equipment, with its standard software (functions of digitization, enhancement, measure,...) adapted to our type of analysis. Turbulent/non-turbulent wake interfaces were identified using the grey level of each pixel as a classifier variable, which decides if the pixel is in or outside the wake.

The first step in processing involved the correction of the inevitable positioning errors produced in the digitization process. This correction was made for each image, automatically comparing reference elements of each frame (position of the cylinder and orientation of the frame edges) with those of one other frame adopted as a pattern. In order to obtain a nearly uniform background, each image was filtered and combined with its corresponding original one by means of the shading correction function implemented on the IBAS/IPS system. Spatial low-pass filters with a very low cut-off frequency (averaging in a window of 50×50 pixels) were used in the illumination correction. After these preprocessing procedures, analysis of the grey-level profiles at each X/D position gave the location of the turbulent/non-turbulent interface.

As an example of the process, figure 4(*a*) shows the preprocessed image corresponding to the frame shown in figure 3(*a*). Figure 4(*b*) contains the grey-level lateral profiles at $X/D = 2$ and 7. For each X/D position analysed, the grey-level profile was transferred to an IBM 3083 computer on which the instantaneous interface position was evaluated. Figure 4(*c*) shows schematically the criterion

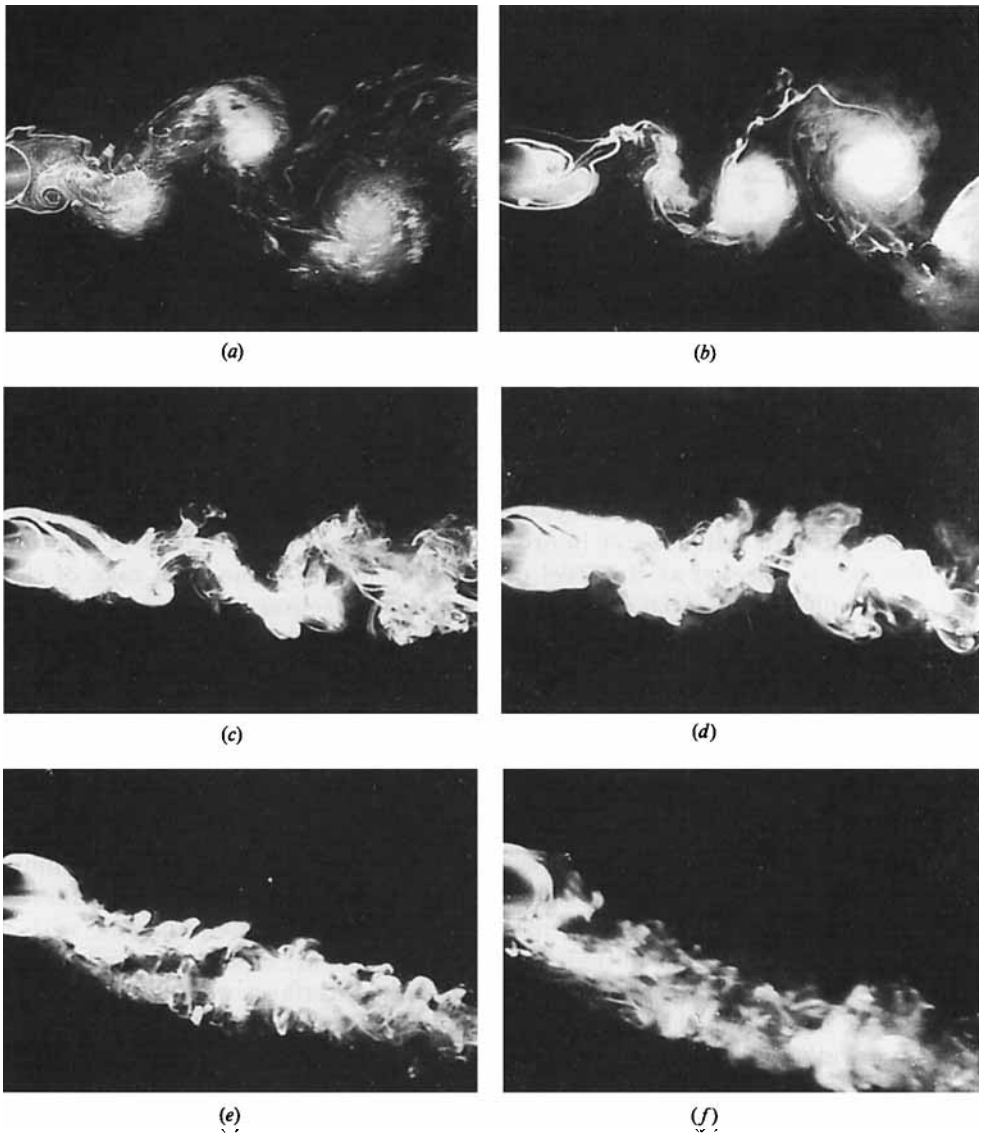

FIGURE 3. Typical frames from the cine film: (a) $\lambda = 0$, (b) 1, (c) 1.5, (d) 2, (e) 3, (f) 4.

adopted to obtain the interface location. In the first stage, the profile was smoothed, averaging the grey value of each pixel with the thirteen nearest ones. After locating the first maximum of the grey-level profile, P in figure 4(c), the instantaneous coordinate of the lower interface of the wake was determined as the Y- value which satisfies

$$\int_{-2.76}^{Y/D} (G - G_0)\,\mathrm{d}Y = \int_{Y/D}^{Y_P/D} (G_P - G)\,\mathrm{d}Y, \tag{1}$$

where Y_P/D is the position of the first maximum of the grey-level profile, G is the grey-level value, G_0 is the background mean grey level and G_P is the grey level at Y_P/D. The position of the upper interface was determined in the same way. This method is not affected by the uniformity defects of the illumination in the

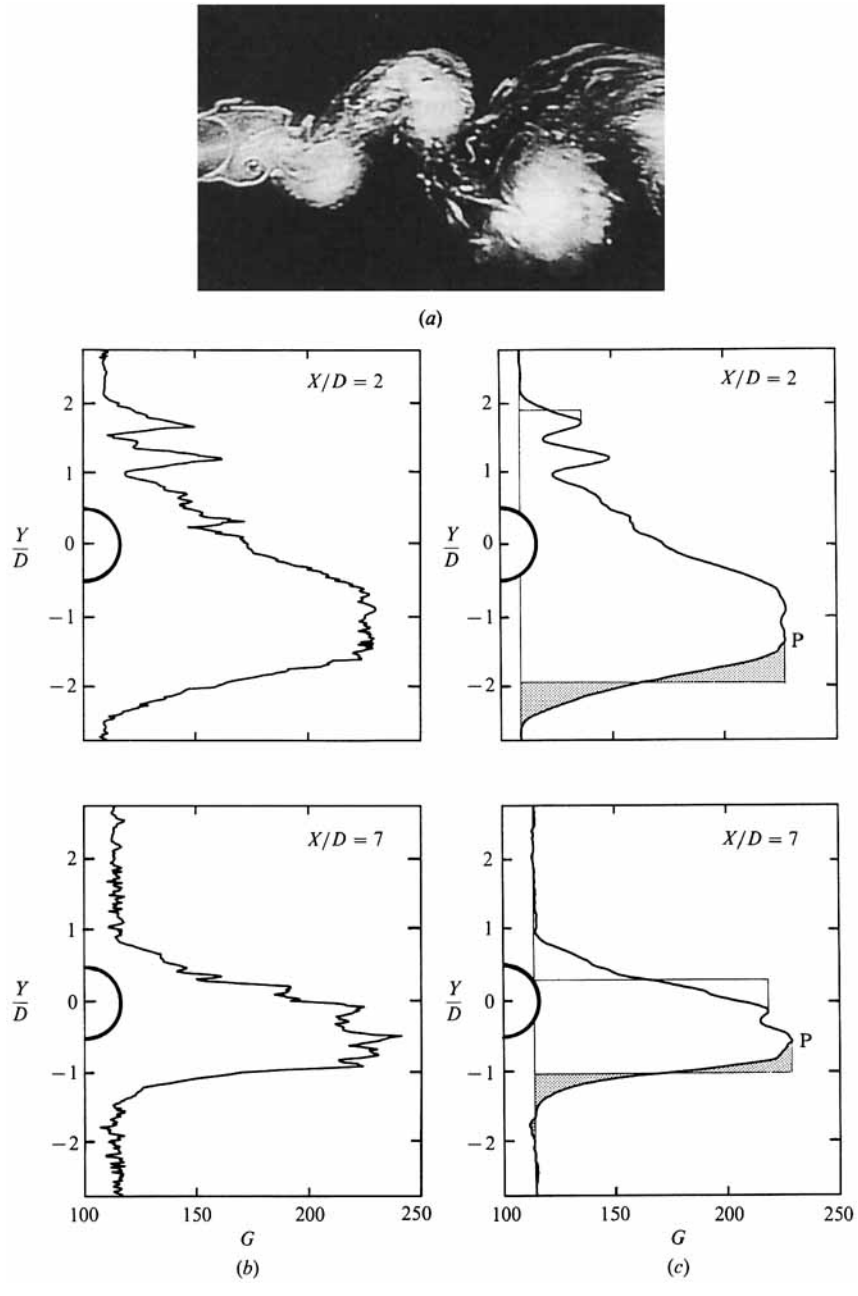

FIGURE 4. Stages for interface location. (*a*) Preprocessed image. (*b*) Grey-level profile at $X/D = 2$, and 7. (*c*) criterion adopted for localizing the interface position on a filtered version of the profile of (*b*).

longitudinal direction, allowing an individual study for each position, and consequently it is more efficient than the ones based on the choice of a global threshold level for the whole image (Shokr, Keffer & Kawall 1983), and at the same time it is faster than the methods that obtain binary images using different local thresholds (Hernán & Jiménez 1982).

4. Analytical details

Results include the mean and r.m.s. interface position, skewness, flatness and the profiles of intermittency and burst rate, auto- and cross-correlation functions, auto- and cross-spectra and phase spectra. The instantaneous lateral position of the interface was separated into its mean and fluctuating value, $Y = \overline{Y} + \tilde{Y}$. The mean value, $\overline{Y}$, is defined as

$$\overline{Y} = \frac{1}{N} \sum_{i=1}^{N} Y(t_i), \tag{2}$$

where N is the number of picture frames examined ($N = 600$) and $Y(t_i)$ is the interface lateral position at $t_i = (i-1)\,\Delta t$, Δt being the time between two consecutive frames in the analysed films ($\Delta t = \frac{1}{24}$ s).

The r.m.s. of the signal, y', which gives statistical information about the averaged intensity of the fluctuating field, is defined as

$$y' = \left[\frac{1}{N} \sum_{i=1}^{N} \tilde{Y}^2(t_i)\right]^{\frac{1}{2}}. \tag{3}$$

The skewness factor, S, which detects the signal asymmetry, is

$$S = \frac{1}{N y'^3} \sum_{i=1}^{N} \tilde{Y}^3(t_i). \tag{4}$$

The flatness factor, K, is defined as

$$K = \frac{1}{N y'^4} \sum_{i=1}^{N} \tilde{Y}^4(t_i). \tag{5}$$

An important parameter of the interface statistics is the intermittency factor, γ, which is defined as the probability of occurrence of turbulent fluid at a specific location (X_0, Y_0). This probability corresponds to the mean value of the indicator function, defined as

$$I(X, Y, t) = \begin{cases} 1 & \text{if turbulent fluid occurs at position } (X, Y) \text{ at time } t \\ 0 & \text{otherwise.} \end{cases} \tag{6}$$

In this work, an equivalent definition is used, which considers the intermittency factor as the probability that the instantaneous interface lateral position is equal to, or higher than, Y_0 at X_0. Consequently, the intermittency factor is calculated as

$$\gamma(Y_0) = \frac{t_{Y \geq Y_0}}{t_{\text{total}}}, \tag{7}$$

where $t_{Y \geq Y_0}$ is the time during which the instantaneous interface position has values equal to, or higher than, Y_0 and t_{total} is the total duration of the cinematographic recording analysed. Figure 5 depicts a scheme for the determination of the intermittency factor, based on the temporal evolution of the interface lateral position at $X = X_0$.

The burst rate, $\hat{f}$, represents the average frequency of occurrence of turbulent eruptions at a given point in the flow and corresponds to the average number of zero-to-unity transitions of the indicator function per unit time. It is calculated as half the average frequency at which the interface crosses a position Y_0. It is usually represented normalized by $\hat{f}_0$, the frequency at which the interface crosses its average position.

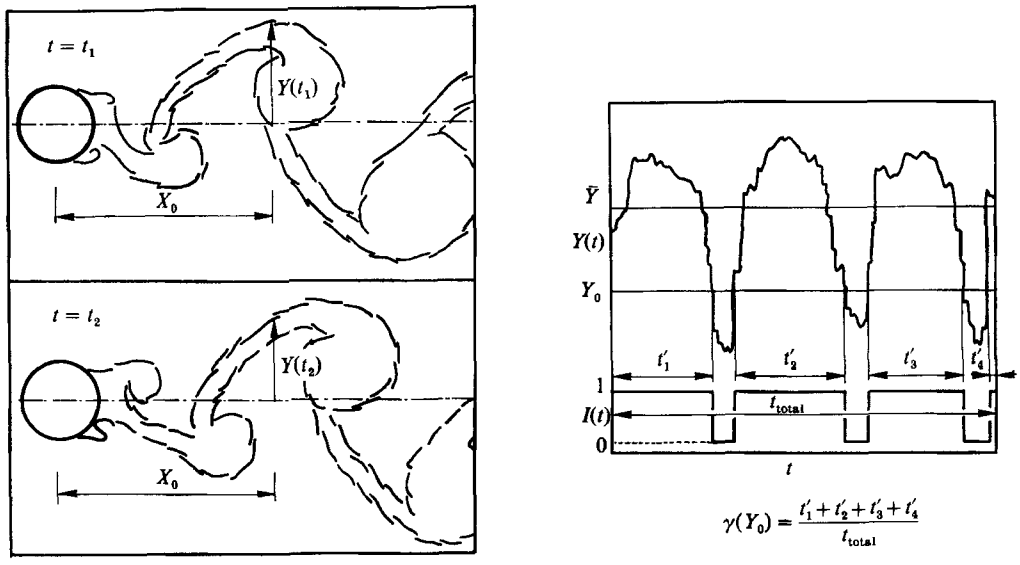

FIGURE 5. Scheme for determination of the intermittency factor.

The auto- and cross-correlation functions $\rho_{nn'}$ are computed as

$$\rho_{nn'}(k\Delta t) = \frac{1}{y'_n y'_{n'}(N-k)} \sum_{j=1}^{N-k} \tilde{Y}_n(t_j)\, \tilde{Y}_{n'}(t_{j+k}), \tag{8}$$

where $k = 0, 1, 2, 3, \ldots, K$ with $K \ll N$ ($K = 300$ in the present calculations). Subscripts n and n' are used to indicate that the variables of the two stations to be correlated correspond to positions $X/D = n$ and n'. If $n = n'$, (8) evaluates the auto-correlation function and if $n \neq n'$ it evaluates the cross-correlation function. The condition $\rho_{nn'}(k\Delta t) = \rho_{n'n}(-k\Delta t)$ is satisfied.

The auto- and cross-spectra are defined from the auto-and cross-correlation functions. These spectra describe the frequency composition of the above-mentioned correlations. These are related by

$$E_{nn'}\left(\frac{k}{M\Delta t}\right) = \left|C_{nn'}\left(\frac{k}{M\Delta t}\right)\right| = \left|\Delta t \sum_{m=-K}^{K} \rho_{nn'}(m\Delta t) \exp\left[-2\pi i m k/M\right]\right|, \tag{9}$$

where $M = 2K+1$. If $n = n'$, this latter relationship leads to the auto-spectrum, and if $n \neq n'$ it yields the modulus of the cross-spectrum. In the present study, the spectral resolution is about 0.04 Hz. The phase with which the different frequencies contribute to the signal is evaluated from the phase spectrum, defined as

$$\phi_{nn'}\left(\frac{K}{M\Delta t}\right) = \arctan\left[\frac{-\mathrm{Im}\left[C_{nn'}(k/M\Delta t)\right]}{\mathrm{Re}\left[C_{nn'}(k/M\Delta t)\right]}\right]. \tag{10}$$

5. Stationary-cylinder results

The longitudinal evolution of the mean value of the interface position of the near wake generated by a stationary cylinder is presented in figure 6. The lateral position

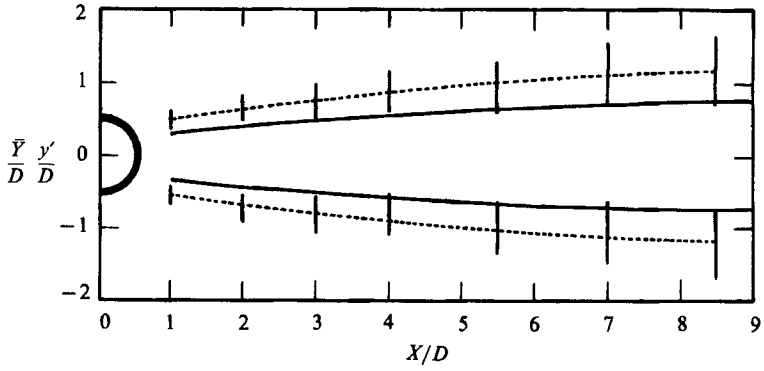

FIGURE 6. Mean and r.m.s. values of the interface position of a stationary cylinder. Mean values are centred on the vertical bars representing r.m.s. values. ——, Béguier *et al.* (1978).

of the interface is non-dimensionalized by the cylinder diameter $\overline{Y}/D$. The vertical bars represent the r.m.s. values, also normalized by the cylinder diameter, y'/D. The values of $\overline{Y}/D$ are compared with the wake width (L_0/D) obtained by Béguier, Giralt & Keffer (1978). We note that both results are consistent and they present a similar tendency in both evolutions. The L_0/D values are lower than the $\overline{Y}/D$ ones because of the different definition of the two variables. L_0 is defined as the lateral half-separation between the points with a velocity defect equal to half the maximum velocity defect. The r.m.s. values behave similarly to the mean value, showing an increase with X/D, in line with the increase of the Kármán vortex size. When the Kármán structures disappear, y'/D decreases with increasing X/D and then the mean velocity profile presents a self-similar form.

As can be seen in figure 7, the longitudinal evolution of the skewness factor for the upper interface of the wake remains roughly constant at around -0.5, showing that the temporal evolution of the interface position in the near wake of a stationary cylinder is a random function with a non-Gaussian behaviour ($S \neq 0$). The positive part of the $Y-\overline{Y}$ signal is significantly different from the negative one (see figure 5). The characteristic geometry of the Kármán vortices establishes that the positive part of this signal remains for longer than the negative one, but the negative one presents higher values of $Y-\overline{Y}$; this implies that the skewness factor is negative for the upper interface. Figure 7 also shows the longitudinal evolution of the skewness factor for the lower interface. It is clear that this evolution presents similar trends to those obtained for the upper interface, with values around 0.5, because of the symmetry of the double Kármán street. The flatness-factor results presented in figure 7 also show a practically constant evolution, with values around 3.1. These values, which are slightly higher than those corresponding to a random Gaussian variable ($K = 3$), indicate that the interface-position signal may be contaminated by high-frequency components, which produce an increase of the ripple in the signal.

Figure 8 shows the profile of the intermittency factor of the upper interface for several longitudinal positions ($X/D = 3$, 4, and 7), as a function of the standardized Gaussian variable, $z = (Y-\overline{Y})/y'$. This figure indicates significant differences between the present results and a Gaussian process, for which

$$\gamma(z) = 1/(2\pi)^{\frac{1}{2}} \int_z^\infty \exp(-\tfrac{1}{2}s^2)\, ds \tag{11}$$

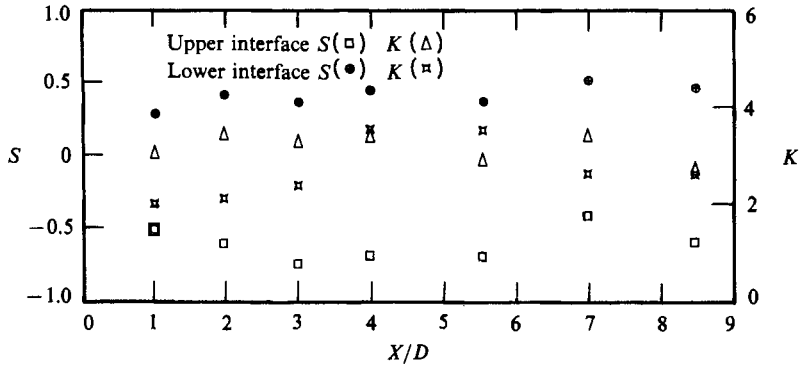

FIGURE 7. Skewness and flatness factors of the interface position of a stationary cylinder.

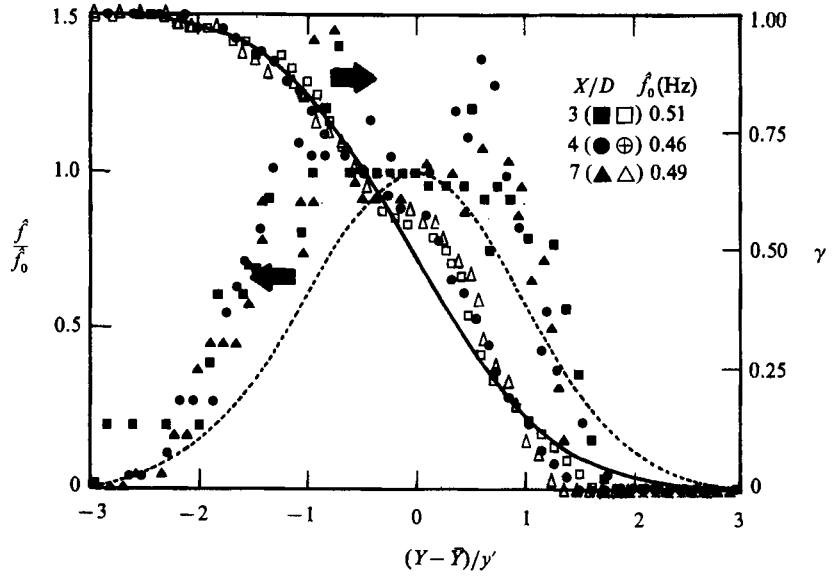

FIGURE 8. Intermittency factor and burst-rate profiles for a stationary cylinder. Open symbols represents intermittency results. Filled symbols represents burst-rate results.

(represented in figure 8 by the solid line). Points located in the upper part of the coherent structures show the maximum differences from Gaussian behaviour, these differences correspond to the skewness (negative value) and flatness (moderate values) factors discussed above. As can be seen in figure 8, the point where $\gamma = \frac{1}{2}$ does not quite coincide with the point $Y = \overline{Y}$. This is related to the higher values of the negative part of the $Y-\overline{Y}$ signal. Consequently, although LaRue & Libby (1976) suggest that the interface position of the fully developed turbulent cylinder wake is a stationary Gaussian random variable, in the near wake the interface presents a clearly non-Gaussian behaviour, because of the presence of the coherent Kármán vortices. Figure 8 also includes the burst-rate profiles. These results also show differences from the relation for a Gaussian process $(\hat{f}(z)/\hat{f}_0 = \exp(-\frac{1}{2}z^2))$, represented by the dashed line. It is clear from this figure that the burst-rate profile would be

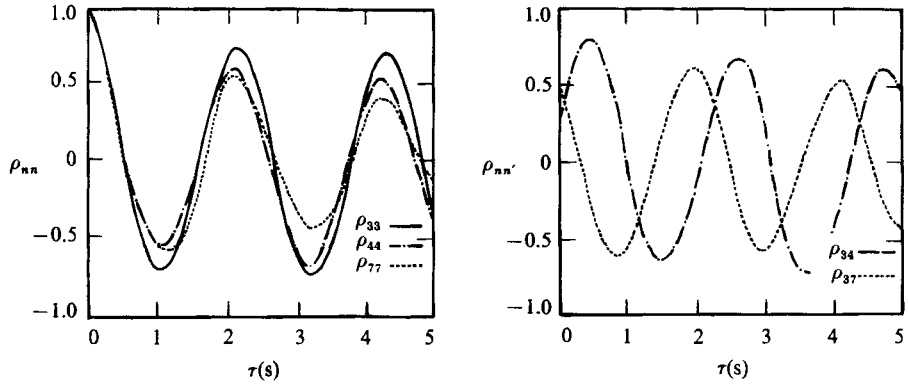

FIGURE 9. Auto- and cross-correlation functions for a stationary cylinder.

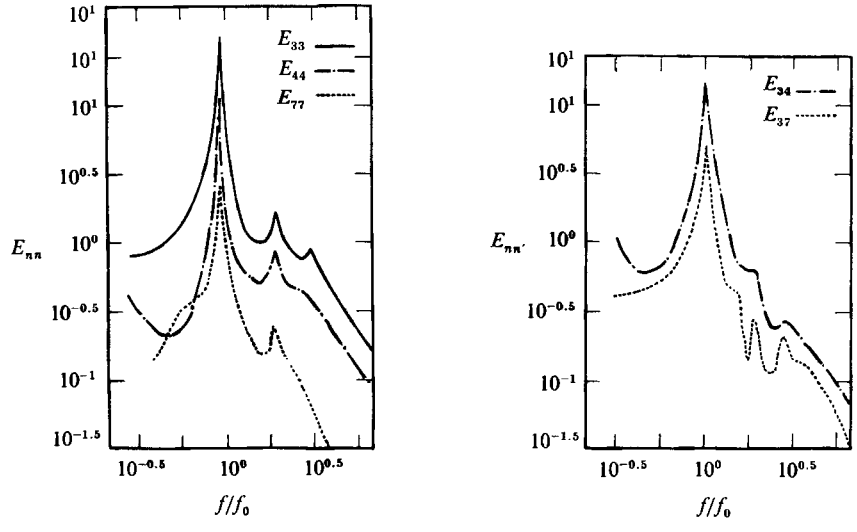

FIGURE 10. Auto- and cross-spectra for a stationary cylinder.

better correlated with a rectangular-shaped function with an amplitude of around 1 and centred at a negative value of $(Y-\overline{Y})/y'$, near to zero. The dominant frequency of the large coherent structures established in this flow, slightly modulated by high-frequency components (harmonics, noise, ...), produces this characteristic behaviour, which induces a sharp decrease of the burst rate for interface positions greater than $(Y-\overline{Y})/y' \approx 1.5$. The value obtained for $\hat{f}_0$ at the analysed positions ($\hat{f}_0 \approx 0.49$ Hz) remains roughly constant in the interval $-1 < (Y-\overline{Y})/y' < 1$, and approximately corresponds to the Strouhal frequency ($f = 0.47$ Hz).

Figure 9 presents the auto-correlation functions at $X/D = 3$, 4 and 7 for the upper interface, shown as ρ_{33}, ρ_{44} and ρ_{77} respectively. Regular oscillations exist, indicating that a well-defined Kármán vortex activity characterizes the near-wake region. The slow but significant decay of the amplitude of the oscillations with increasing τ shows that the vortex shedding process is randomly modulated in frequency and phase, as established by Budny, Kawall & Keffer (1979). This decay increases as X/D increases, as a result of the gradual diffusion of the vortices. The dominant frequency

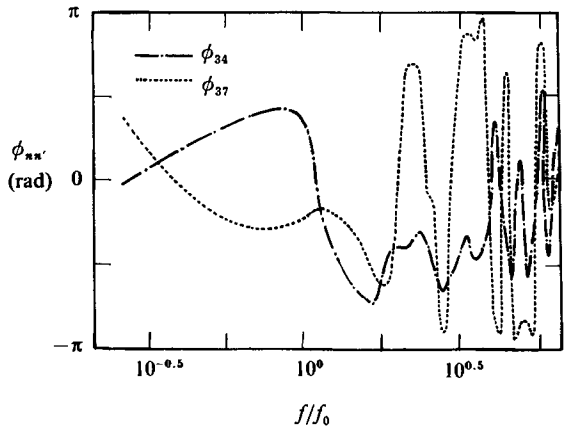

FIGURE 11. Phase spectra for a stationary cylinder.

associated with this function is $f_0 = 0.48$ Hz, which gives an accurate determination of the vortex shedding frequency. The value of the Strouhal number associated with this characteristic frequency is about 0.22, in good agreement with the results found by Díaz *et al.* (1983) using hot-wire anemometry. Streamwise cross-correlation functions ρ_{34} and ρ_{37} are also presented in figure 9. These results establish that the decay of the amplitude of the oscillations increases with increasing distance between the two correlated stations. The lag-time values corresponding with the first maxima of these functions are in agreement with the distance between stations and the free-stream velocity.

Figure 10 presents the auto-spectra and the moduli of the cross-spectra obtained from the auto- and cross-correlation functions. All the spectra confirm the periodic behaviour of the signals, already mentioned. A well-defined peak, which is related to the shedding frequency of Kármán vortices, exists at 0.48 Hz. As can be seen, the different spectra show the presence of two harmonics, signifying that their energetic contribution is relevant in the wake. Phase spectra ϕ_{34} and ϕ_{37} are presented in figure 11. It can be seen that these values are consistent with the behaviour of the cross-correlation functions obtained. It can also be observed that no coherent contributions to the signal exist for frequencies greater than $3f_0$.

6. Spinning-cylinder results

The statistical analysis developed for the stationary-cylinder near wake is extended to the spinning-cylinder case. Visualizations of the flow generated in the near wake of a rotating cylinder with peripheral speeds up to 4 times the free-stream velocity were carried out. Statistical results corresponding to $\lambda \equiv U_p/U_0 = 1.5, 2$ and 3 are presented here, because they show the most significant modifications introduced by the cylinder rotation.

Figure 12 shows the longitudinal evolution of the mean and r.m.s. values of the upper and lower interface position, both normalized with respect to the cylinder diameter, for $X/D \leqslant 8.5$. It is clear that as λ increases, the near wake is progressively displaced downward and becomes distinctly curved, which is consistent with the fact that a spinning cylinder located in a uniform stream produces a lift force that increases as U_p increases. The wake width decreases as λ increases. Figure 12 also

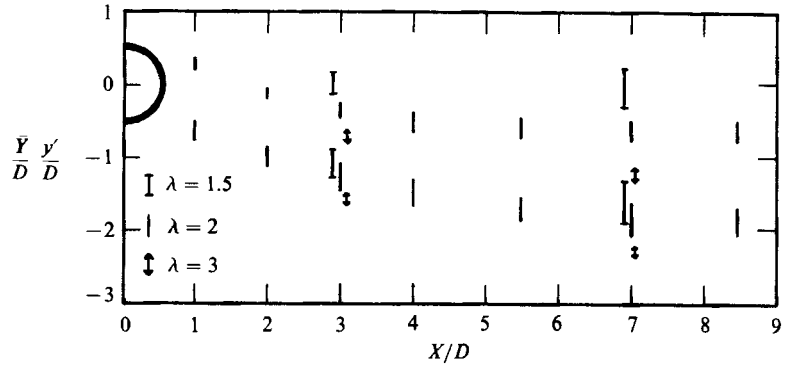

FIGURE 12. Mean and r.m.s. values of the interface position of a rotating cylinder. Mean values are centred on the vertical bars representing r.m.s. values.

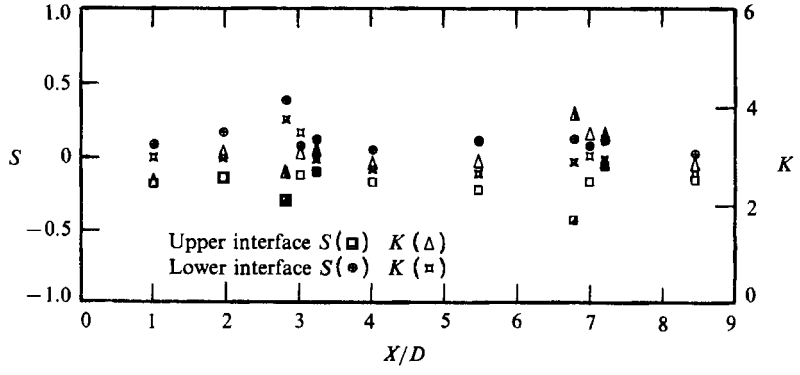

FIGURE 13. Skewness and flatness factors of the interface position of a rotating cylinder: ◪ ◭ ◓ ⧓, λ = 1.5; □ △ ⊕ ⌑, λ = 2; ■ ▲ ● ⧓, λ = 3.

depicts the effect of λ on the fluctuating field. The r.m.s. value of the interface position is lower than the stationary-cylinder case, especially for λ = 2 and 3. These results are entirely consistent with those obtained by Díaz *et al.* (1983), which establish that the dominant feature of a near cylinder wake, i.e. the Kármán vortex activity, diminishes substantially for λ ⩾ 1.5. It is apparent from figure 12 that, at a given station, the r.m.s. value is higher in the lower interface than in the upper one. At the top of the cylinder, the peripheral velocity is in the same direction as the free-stream velocity, consequently boundary-layer separation and vortex shedding are inhibited. At the bottom of the cylinder, the flow velocity and the peripheral speed are opposite and consequently boundary-layer separation is favoured. Visualizations of the near wake using particle tracers (Massons 1987) confirm this.

The longitudinal evolution of the skewness and flatness factors for X/D up to 8.5 is illustrated in figure 13. The skewness values are lower than those corresponding to the stationary-cylinder case, this decrease confirming the tendency toward Gaussian behaviour as rotation velocity increases. Flatness-factor results depict values similar to those obtained for a stationary cylinder. As a consequence of the flow homogenization, an increasing uniformity of skewness and flatness values at different stations is observed.

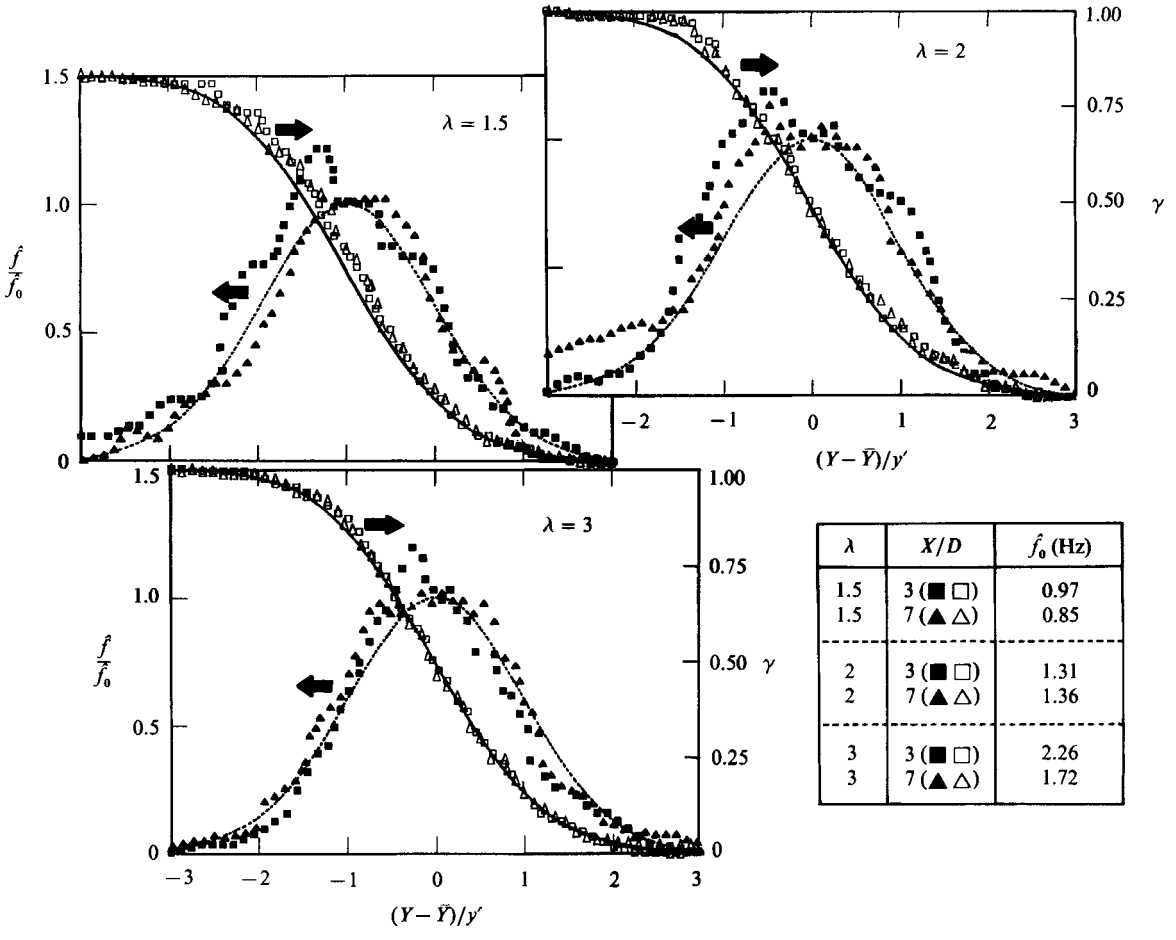

λ	X/D	$\hat{f}_0$ (Hz)
1.5	3 (■ □)	0.97
1.5	7 (▲ △)	0.85
2	3 (■ □)	1.31
2	7 (▲ △)	1.36
3	3 (■ □)	2.26
3	7 (▲ △)	1.72

FIGURE 14. Intermittency factor and burst-rate profiles for a rotating cylinder. Open symbols representing intermittency results. Filled symbolds represents burst-rate results.

Figure 14 shows the intermittency and the burst-rate profiles for the upper interface of the wake at $X/D = 3$ and 7. The distribution for a Gaussian random variable are also included. The results for the intermittency factor are in accordance with the statistical moments, showing that the position of the point having an intermittency factor of $\frac{1}{2}$ is near the mean position of the interface. The burst-rate profile shows the inhibition produced by the solid rotation on the shedding process of the coherent structures. As λ increases, the intermittency and the burst-rate profiles show a clear evolution toward Gaussian behaviour. For $\lambda = 3$, the experimental results agree well with the Gaussian functions, indicating that the process becomes partially Gaussian as no significant structures are shed from the cylinder.

Figure 15 shows the auto- and cross-correlation functions obtained at $X/D = 3$ and 7 for the upper interface. These functions show oscillations whose amplitude decreases as the peripheral velocity increases and the Kármán vortex activity diminishes. The oscillatory character of these functions decreases sharply as λ increases. The dominant role of the Kármán coherent structures, shown in the

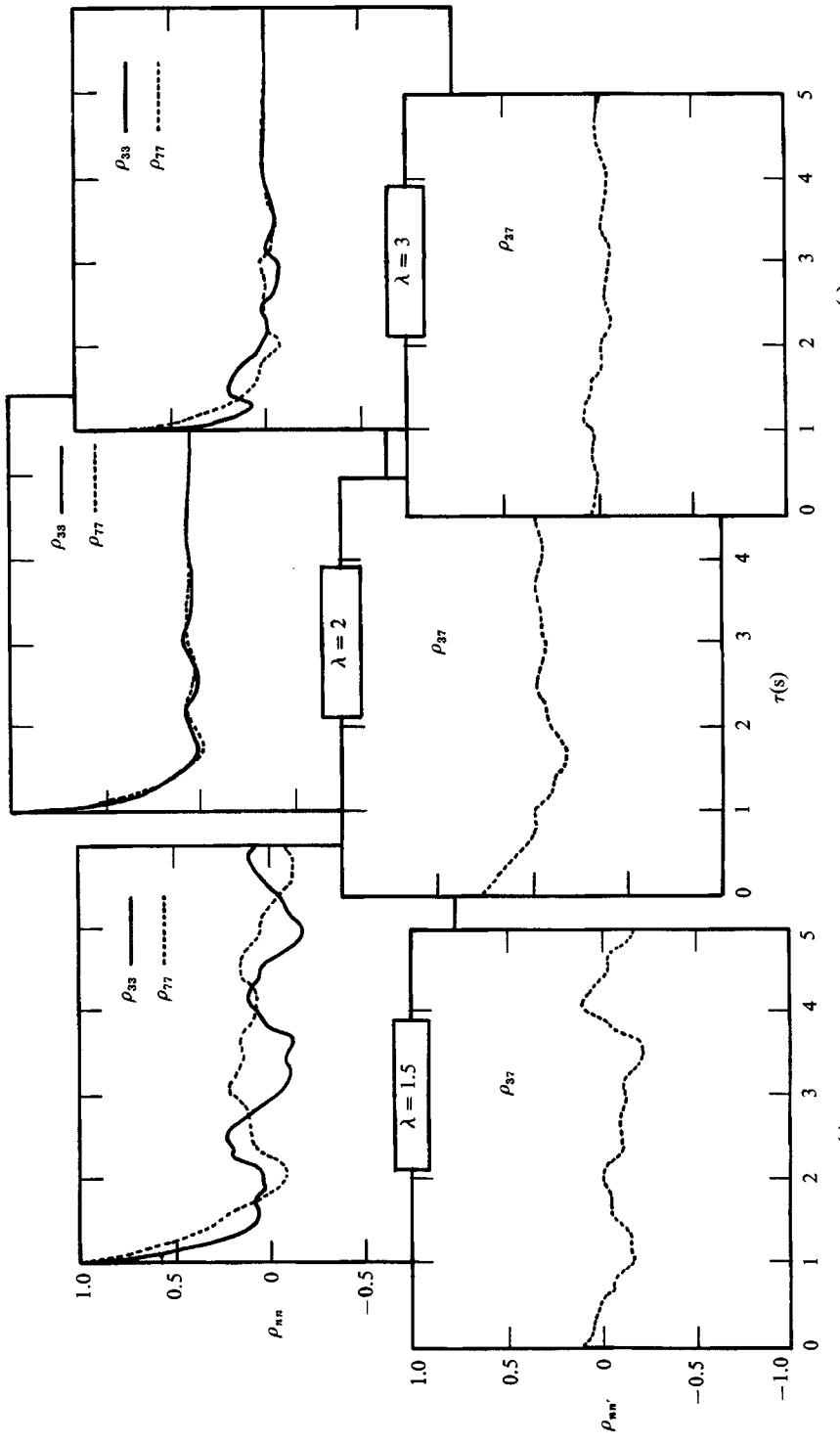

FIGURE 15. Auto- and cross-correlation functions for a rotating cylinder.

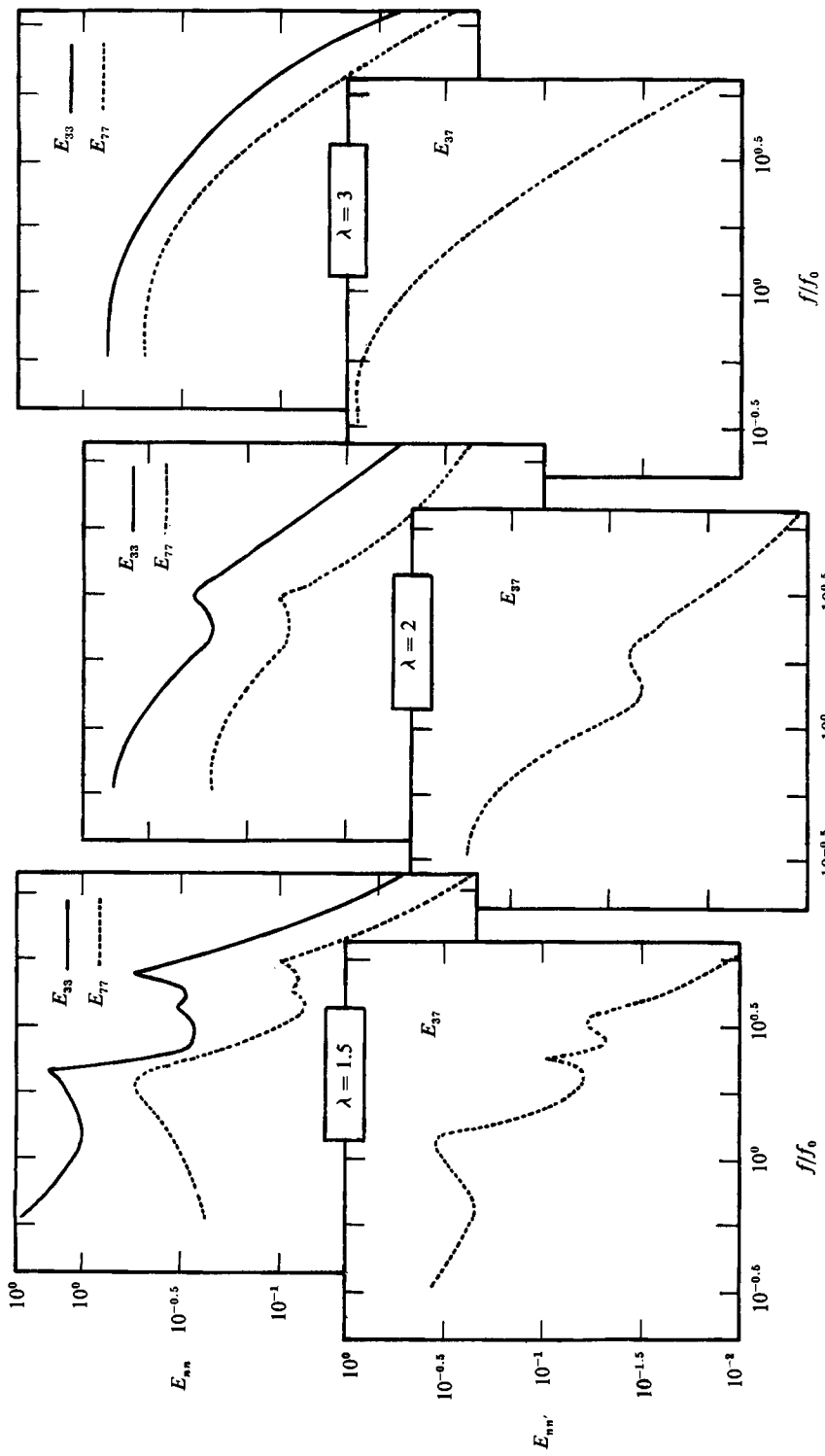

FIGURE 16. Auto- and cross-spectra for a rotating cylinder.

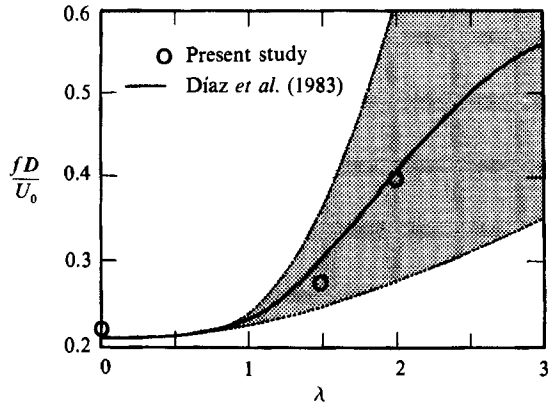

FIGURE 17. Evolution of Strouhal number with λ.

stationary cylinder case, does not exist for the spinning cylinder case. For $\lambda \approx 1.5$ the mean velocity profiles at the top and the bottom of the cylinder are completely asymmetrical (Díaz *et al.* 1983) and vortex shedding is increasingly inhibited, producing a redistribution of the kinetic energy over all relevant structures of the flow.

The frequency analysis of the flow is shown in figure 16. The auto-spectra and the moduli of the cross-spectra for $\lambda = 1.5, 2$ and 3 are presented. The results prove that, as a result of the homogenization produced in the flow by the cylinder rotation, the spectral peaks becomes substantially lower than those observed in the stationary case. The nominal frequency at which the fundamental peaks occur is $f = 0.60$ Hz (Strouhal number $St = 0.27$) and $f = 0.87$ Hz ($St = 0.39$) for $\lambda = 1.5$ and 2, respectively. For $\lambda = 3$, the spectra displays no such peak, indicating that the shedding process becomes completely random. The variation of the Strouhal number with λ is shown in figure 17, together with comparison of the present results and those of Díaz *et al.* (1983). For $\lambda \geqslant 1.5$, a specific Strouhal number cannot be defined from the spectral results because the peaks are broadband as a consequence of the sharp increase of the random modulation in the shedding process, as indicated in figure 17 by the shaded area.

7. Conclusions

The time evolution and statistical properties of the turbulent/non-turbulent interface position in the near wake generated by stationary and spinning cylinders has been studied by digital analysis of cinematographic records of dye injection.

The symmetrical shape of the stationary cylinder wake and its structure deduced from the statistical moments of the interface position is distorted by the cylinder rotation. The peripheral velocity of the cylinder introduces a progressive lateral deflection of the wake. The conventional Kármán vortex shedding is modified by rotation and for $\lambda \geqslant 1.5$ a significant inhibition is produced. The gradual homogenization of the flow causes a reduction of the wake width. At the same time, a pronounced evolution towards Gaussian behaviour is favoured by the absence of well-defined structures. Frequency analysis shows that the shedding frequency increases with an increase of the rotation speed, and becomes more undefined (broadband peak).

The authors would like to thank the 'Jaime Almera' Institute, CSIC, for the loan of the image processing equipment. The financial support provided by CIRIT (Generalitat de Catalunya) and the technical facilities provided by Taqsa and Repsol Petroleo, S.A. are also acknowledged.

REFERENCES

ANTONIA, R. A. & BRADSHAW, P. 1971 Conditional sampling of turbulent shear flows. *Imperial College Aeronaut. Rep.* 71–04.

BÉGUIER, C., GIRALT, F. & KEFFER, J. F. 1978 Turbulent heated flows with asymmetrical mean temperature profiles. *Proc VI Intl Heat Transfer Conference, Toronto.*

BROWNE, L. W. B. & ANTONIA, R. A. 1986 Reynolds shear stress and heat flux measurements in a cylinder wake. *Phys. Fluids* **29**, 709–713.

BUDNY, R. S., KAWALL, J. G. & KEFFER, J. G. 1979 Vortex street evolution in the wake of a circular cylinder. *Proc. 2nd. Intl Symp. on Turbulent Shear Flows. Imperial College. London.*

CHARRIER, B. 1979 Etude théorique et experimentale de l'effect Magnus destiné à la propulsion des navires. Thesis. University of Paris VI.

DÍAZ, F., GAVALDÀ, J., KAWALL, J. G., KEFFER, J. F. & GIRALT, F. 1983 Vortex shedding from a spinning cylinder. *Phys. Fluids* **26**, 3454–3460.

DÍAZ, F., GAVALDÀ, J., KAWALL, J. G., KEFFER, J. F. & GIRALT, F. 1985 Asymmetrical wake generated by a spinning cylinder. *AIAA J.* **23**, 49–54.

EATON, B. E. 1987 Analysis of laminar vortex shedding behind a circular cylinder by computer-aided flow visualization. *J. Fluid Mech.* **180**, 117–145.

FREYMUTH, P., FINAISH, F. & BANK, W. 1986 Visualization of the vortex street behind a circular cylinder at low Reynolds numbers. *Phys. Fluids* **29**, 1321–1323.

GERRARD, J. H. 1966 The mechanics of the formation region of vortices behind bluff bodies. *J. Fluid Mech.* **25**, 401–413.

HERNÁN, M. A. & JIMÉNEZ, J. 1982 Computer analysis of a high-speed film for a turbulent mixing layer. *J. Fluid Mech.* **119**, 323–345.

HESSELINK, L. 1988 Digital image processing in flow visualization. *Ann. Rev. Fluid Mech.* **20**, 421–485.

HESSELINK, L. & WHITE, B. S. 1983 Digital image processing of flow visualization photographs. *Appl. Opt.* **22**, 1454–1461.

JACKSON, C. P. 1987 A finite-element study of the onset of vortex shedding in flow past variously shaped bodies. *J. Fluid Mech.* **182**, 23–45.

KEFFER, J. F. 1965 The uniform distortion of a turbulent wake. *J. Fluid Mech.* **22**, 135–159.

KOBAYASHI, T., YOSHITAKE, Y., SAGA, T. & SEGAWA, S. 1985 An image processing technique for determining two dimensional flow fields with reverse flow. In *Proc. Intl Symp. on Physical and Numerical Flow Visualization* (ed. M. L. Billet, J. H. Kim & T. R. Heidrick), pp. 39–46. ASME.

KOURTA, A., BOISSON, H. C., CHASSAING, P. & HA MING, H. 1987 Nonlinear interaction and the transition to turbulence in the wake of a circular cylinder. *J. Fluid Mech.* **181**, 141–161.

LARUE, J. C. & LIBBY, P. A. 1976 Statistical properties of the interface in a turbulent wake of a heated cylinder. *Phys. Fluids* **19**, 1864–1875.

LIM, C. C. & SIROVICH, L. 1986 Wave propagation on the von Kármán trail. *Phys. Fluids* **29**, 3910–3911.

MARKO, K. A. & RIMAI, L. 1985 Video recording and quantitative analysis of seed particle track images in unsteady flows. *Appl. Opt.* **24**, 3666–3672.

MASSONS, J. 1987 Processat digital d'imatges aplicat a l'anàlisi de la generació i establiment de l'estela d'un cilindre. Thesis. University of Barcelona.

MASSONS, J., ESCODA, J., GAVALDÀ, J. & DÍAZ, F. 1986 Image analysis of the spinning cylinder near wake. In *Advances in Turbulence* (ed. G. Comte-Bellot & J. Mathieu), pp. 508–513. Springer.

NAGIB, H., CORKE, T., HILLAND, K. & WAY, J. 1979 Computer analysis of flow visualization records obtained by the smoke-wire technique. In *Proc. Dynamic Flow Conference 1978* (ed. L. S. G. Kovasznay, A. Faure, P. Buchhave & L. Fulachier), pp. 567–581.

PRASAD, R. R. & SREENIVASAN, K. R. 1989 Scalar interfaces in digital images of turbulent flows. *Exps Fluids* (in press).

RAJAGOPALAN, S. & ANTONIA, R. A. 1981 Properties of the large structure in slightly heated turbulent mixing layer of a plane jet. *J. Fluid Mech.* **105**, 261–281.

ROSHKO, A. 1953 On the development of turbulent wakes from vortex streets. *NACA Tech. Note* 2913.

SADJADI, F. A., WAND, J. J., HALL, E. L. & ROBERTS, M. J. 1980 Measurement of two phase flow using image correlation. *Proc. 5th Intl Conf. of Pattern Recognition, Miami Beach, Florida.*

SCHLIHTING, H. 1958 *Boundary Layer Theory*. McGraw-Hill.

SHOKR, M. & KEFFER, J. F. 1982 Digital image analysis of a complex turbulent wake. In *Structure of Complex Turbulent Shear Flow* (ed. R. Dumas & L. Fulachier), pp. 165–174. Springer.

SHOKR, M., KEFFER, J. F. & KAWALL, J. G. 1983 Structural features of the near region of an asymmetric turbulent wake. *Proc. IVth Symp. on Turbulent Shear Flows. Karlsruhe.*

SREENIVASAN, K. R. & TAVOULARIS, S. 1980 On the skewness of the temperature derivative in turbulent flows. *J. Fluid Mech.* **101**, 783–795.

THOMAS, R. M. 1973 Conditional sampling and other measurements in a plane turbulent wake. *J. Fluid Mech.* **57**, 549–582.

TOWNSEND, A. A. 1949 The fully developed turbulent wake of a circular cylinder. *Austral. J. Sci. Res.* A **2**, 451–468.

TRITTON, D. J. 1959 Experiments on the flow past a circular cylinder at low Reynolds numbers. *J. Fluid Mech.* **6**, 547–564.